Supplement of Atmos. Chem. Phys., 20, 13023–13040, 2020
https://doi.org/10.5194/acp-20-13023-2020-supplement

Atmospheric Chemistry and Physics
Open Access

Supplement of

The promotion effect of nitrous acid on aerosol formation in wintertime in Beijing: the possible contribution of traffic-related emissions

Yongchun Liu et al.

Correspondence to: Yongchun Liu (liuyc@buct.edu.cn), Weigang Wang (wangwg@iccas.ac.cn),
and Markku Kulmala (markku.kulmala@helsinki.fi)

Supplement information

Non-refractory $PM_{2.5}$ (NR-$PM_{2.5}$) measurement. Concentration of NR-$PM_{2.5}$ was measured with a ToF-ACSM (Aerodyne Co. Ltd., USA). The operation protocol and the configuration of ToF-ACSM has been described well in previous work (Fröhlich et al., 2013). Namely, $PM_{2.5}$ particles from the inlet were focused by a $PM_{2.5}$ aerodynamic lens (Williams et al., 2013), and then vaporized by a standard vaporizer heated at 600 °C followed by electronic ionization (EI, 70 eV). The non-refractory components including chloride, nitrate, sulfate, ammonia and organics were measured using a time-of-flight mass spectrometer with unit mass resolution (UMR). The concentrations of the above species were calculated based on the measured fragments signals, the signal ions (SI), the fragment table, the measured ionization efficiency (IE) of nitrate and the corresponding relative ionization efficiency (RIE) for sulfate, chloride, ammonia and organics. IE calibration of nitrate was performed using 300 nm dry NH_4NO_3 every month during this observation study.

VOCs measurement. VOCs were measured using a Single Photo Ionization Time-of-flight Mass spectrometer (SPI-ToF-MS 3000R, Hexin Mass Spectrometry). 0.8 L min^{-1} of filtered air was sucked from the whole sampling tube and heated to 80 °C in the inlet. VOCs were selectively enriched continuously through a polydimethylsiloxane (PDMS) membrane, and then ionized by VUV light (10.5 eV) with a deuterium lamp. The concentration of VOCs was determined with the time-of-flight mass spectrometer (ToF-MS) based upon external standard curves of PAMS and TO-15 standard gases (Linde Electronics & Specialty Gases, USA). VOCs with m/z from 40 to 300 were recorded with 3 min of time resolution, while hourly averaged concentration were reported in this work. Calibration was performed every week.

HONO measurement. HONO in ambient air directly sampled from the window of the laboratory was absorbed by a solution containing 0.06 mol L^{-1} sulfnilamide in 1 mol L^{-1} HCl, and then transformed into an azo dye by *N*-(1-naphthyl) ethylene-diaminedihydrochloride (0.8 mml L^{-1}). The azo dye was pumped into Teflon absorption cells (Liquid Core Waveguide, LCW) and detected by a mini-spectrometer with a diode array detector (Ocean Optics, SD2000). The HONO concentrations was obtained by subtracting the calibrated signal of the second coil from the first coil using external nitrile standard solutions. Zero point calibration was performed every day using scrubbed zero air (Tong et al., 2016).

Photolysis rate constants of HONO and O_3. Photolysis rate constants of NO_2(J_{NO2}), HONO(J_{HONO}) and O_3(J_{O3}) under clear sky conditions were calculated according to the solar zenith angle and the location using a box model (FACSIMILE 4). NO_2 photolysis sensor (J_{NO2}, Metcon) was unavailable, while UVB is always available during our observation study. However, it was available from Aug 17 to Sep 16, 2018. A calibration function between the measured UVB light intensity and J_{NO2} was established to correct the influence the climatological O_3 column, aerosol optical depth and cloud cover on surface UV light intensity from Aug 17 to Sep 16, 2008. As shown in Figure S10, the model well predicted the J_{NO2}. Then the J_{NO2} during this campaign study was predicted using the model. We further confirmed the calculated J_{NO2} by comprising the OH concentration estimated by the J_{O1D} according to the equation (c_{OH}=J_{O1D}×2×10^{11}

molecules cm^{-3}) (Tan et al., 2019) and the measured OH concentration at Huairou, which is 60 km northeast from BUCT, form Jan 11 to Mar 10, 2016. As shown in Figure S10C, the estimated diurnal curve of OH is comparable with that measured at Huairou.

Fig. S7 shows the calculated photolysis rates.

Supplementary figures

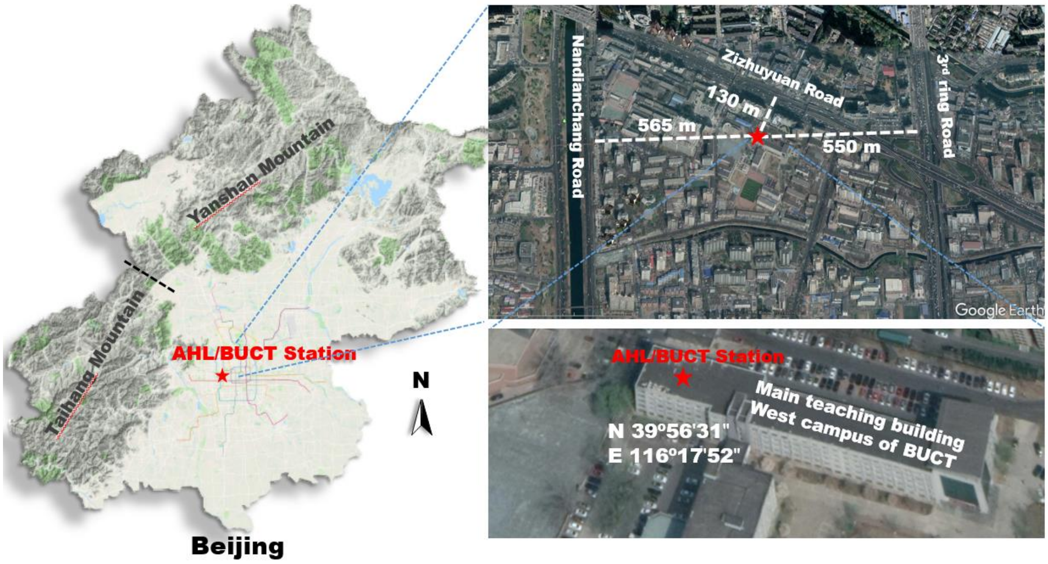

Figure S1. Location of AHL/BUCT observation station. The map was made from Wemap and © Google Earth.

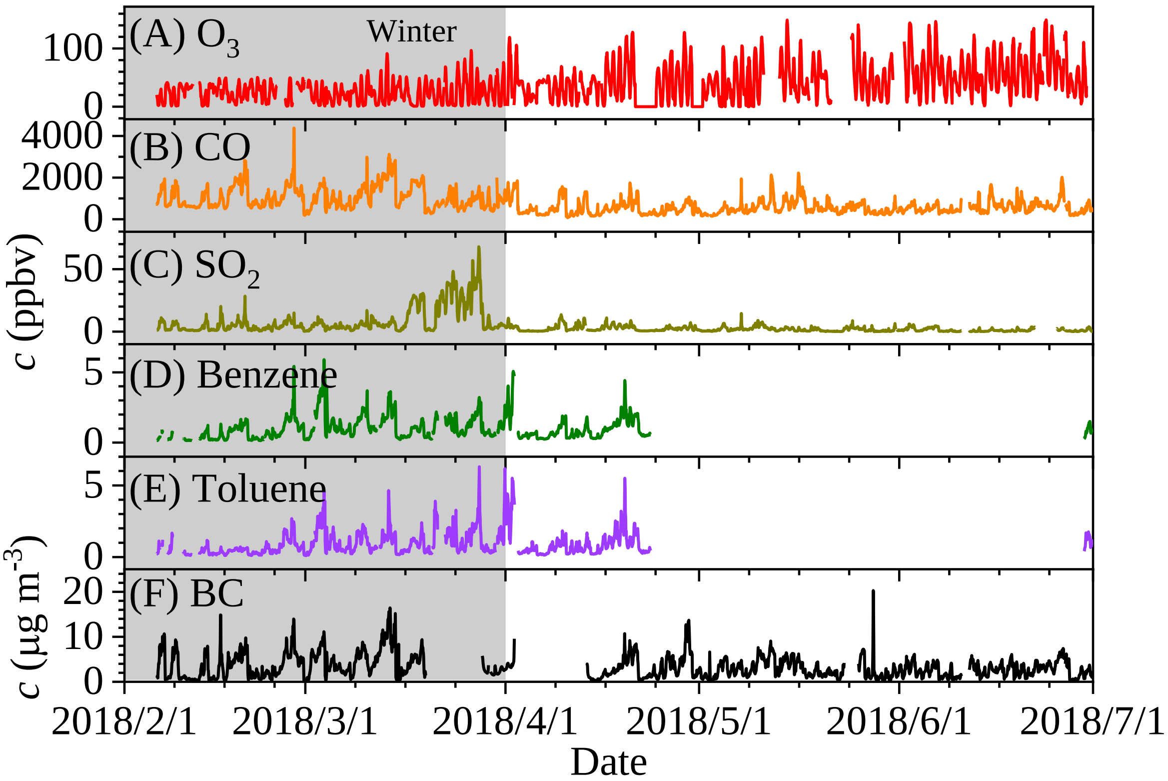

Figure S2. Hourly averaged (A)-(F) concentration of pollutants from Feb 1 to Jun 30, 2018.

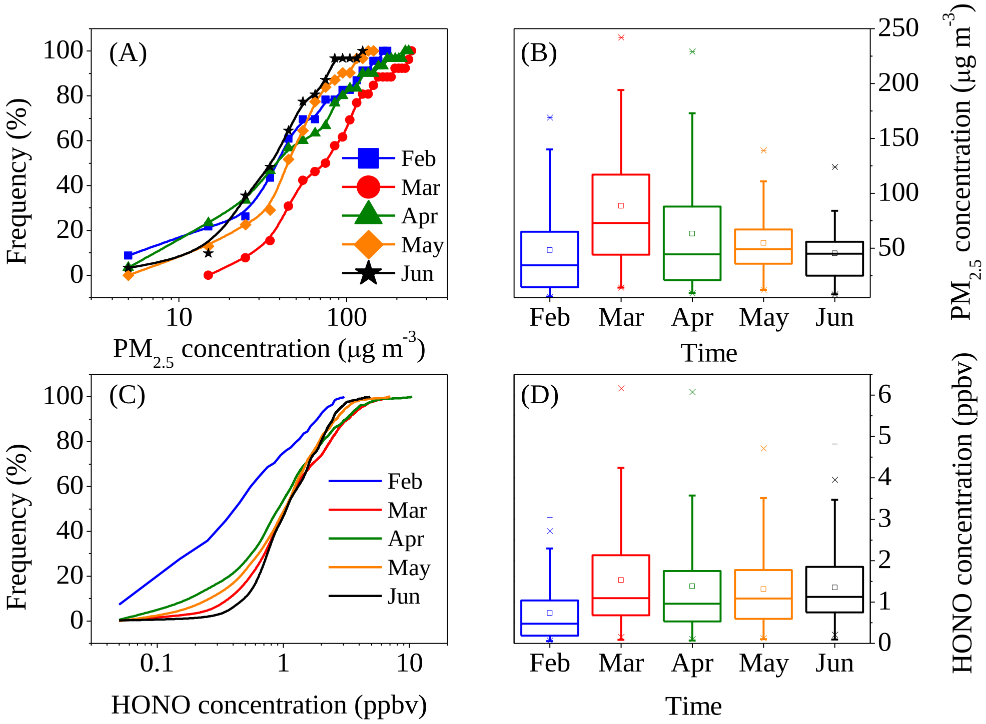

Figure S3. The monthly cumulative frequency of $PM_{2.5}$ and HONO and the monthly mean concentration of $PM_{2.5}$ and HONO.

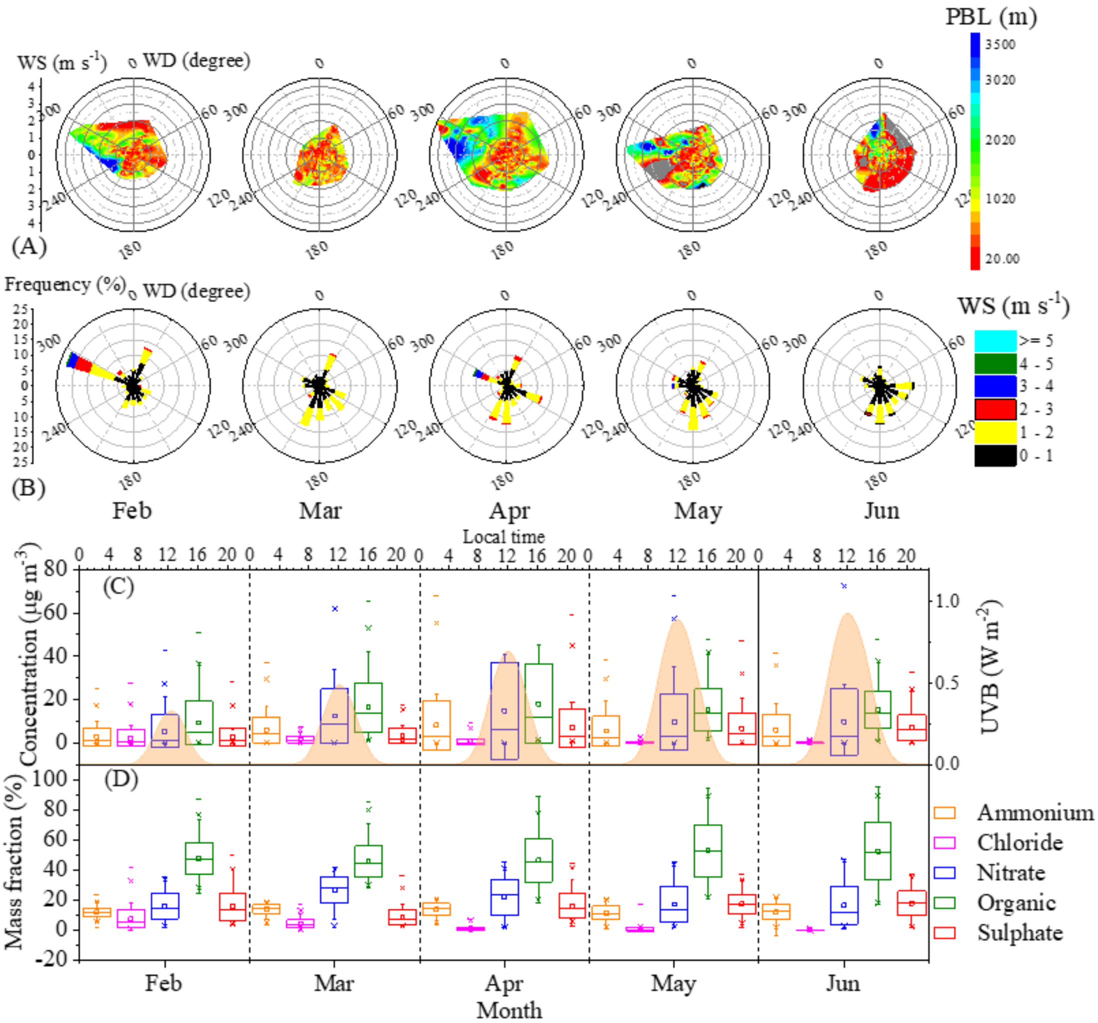

Figure S4. (A)-(B) monthly Windrose-PBL plots, and monthly averaged (C) UVB intensity, mass concentration and (D) fraction of individual component in NR-$PM_{2.5}$ composition from Feb to Jun, 2018.

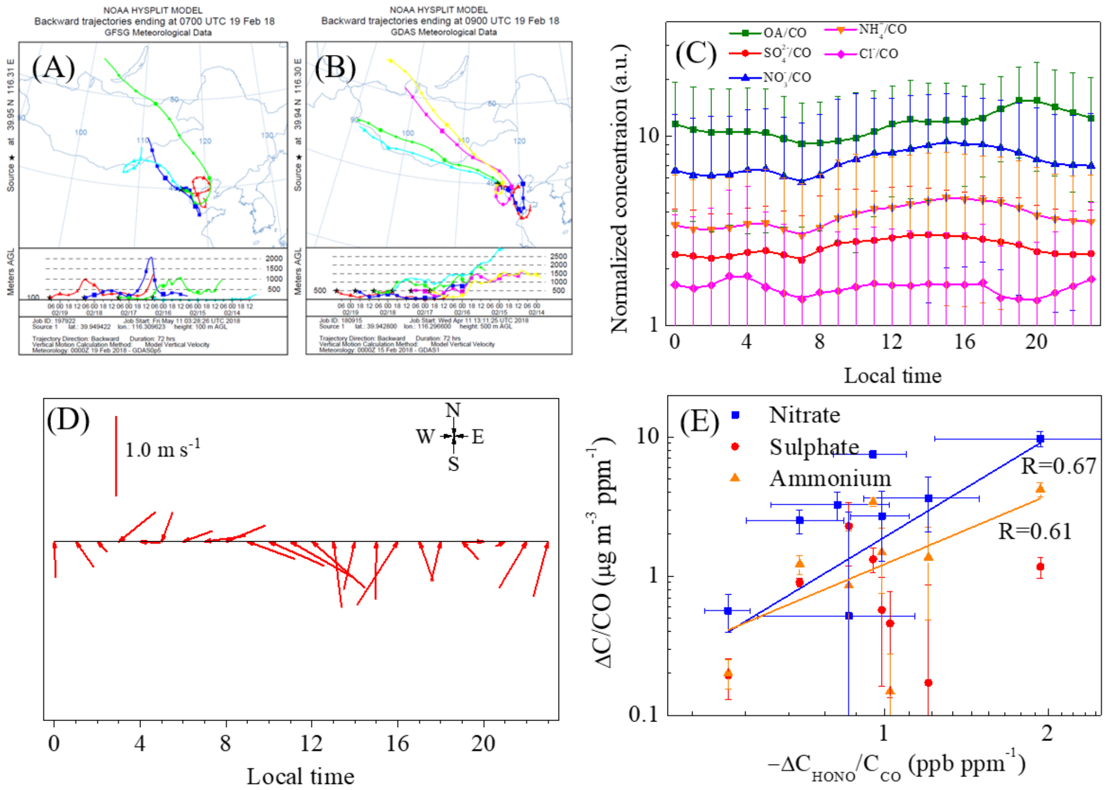

Figure S5. Transport of air mass during Chinese New Year based on back trajectory analysis (A) at 100 and (B) 500 m height; (C) Diurnal variation of NR-$PM_{2.5}$ normalized to CO concentration from Feb 1 to March 31; (D) Hourly averaged wind speed variation in the 12^{th} episode; (E) Correlation of the concentration increment of individual component and consumed HONO normalized to CO in the daytime.

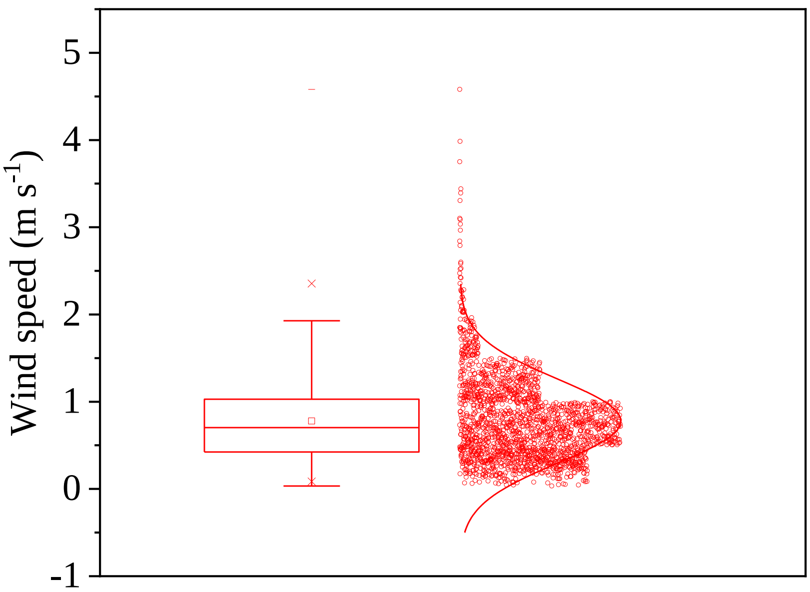

Figure S6. Distribution of wind speed when the $PM_{2.5}$ concentration was larger than 50 μg m^{-3} and the RH was less than 90 %.

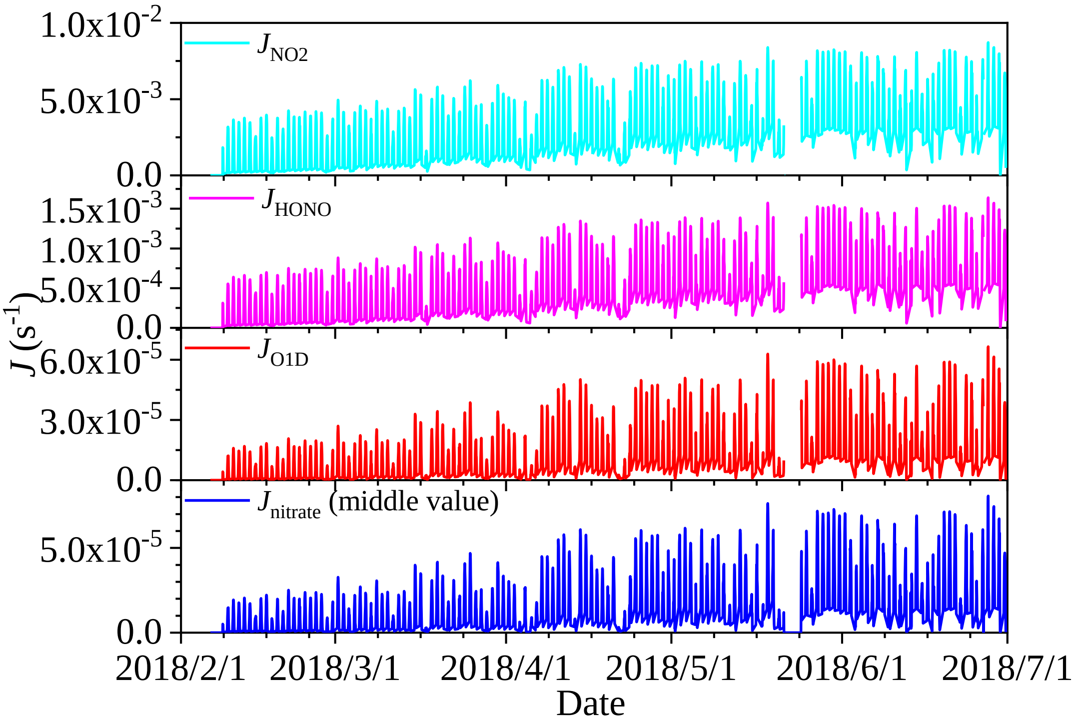

Fig. S7. The photolysis rate of NO_2, HONO, O_3 (O1D) and nitrate (middle value) from 8:00 am to 6:00 pm.

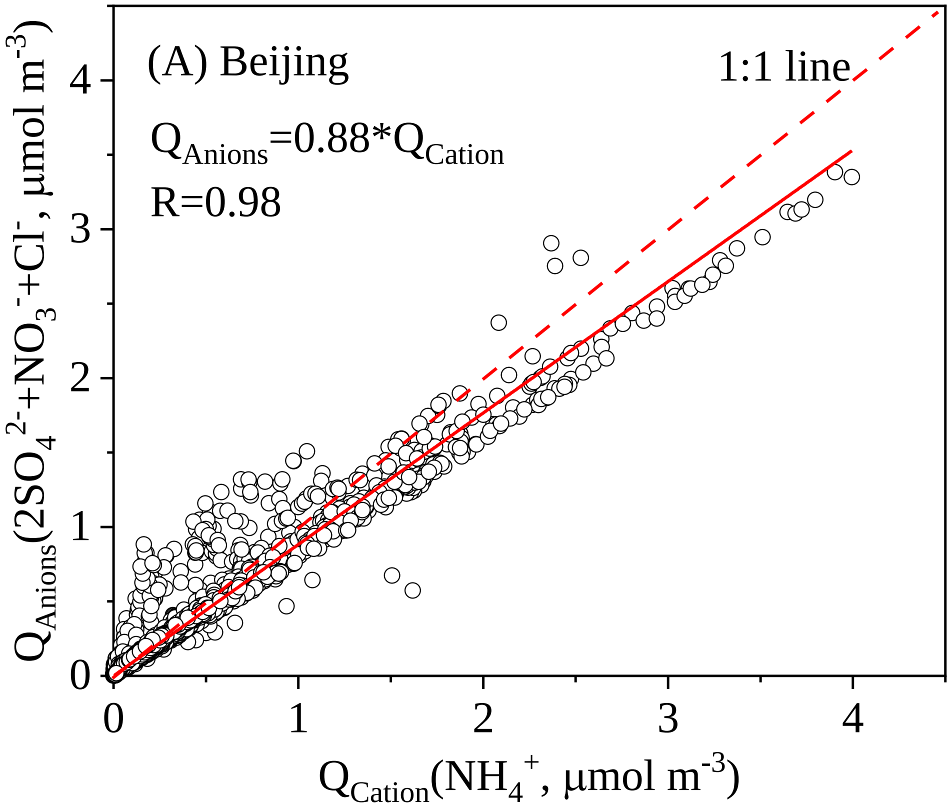

Figure S8. Correlation of the charge between inorganic anions and cations in non-refractory $PM_{2.5}$ in Beijing.

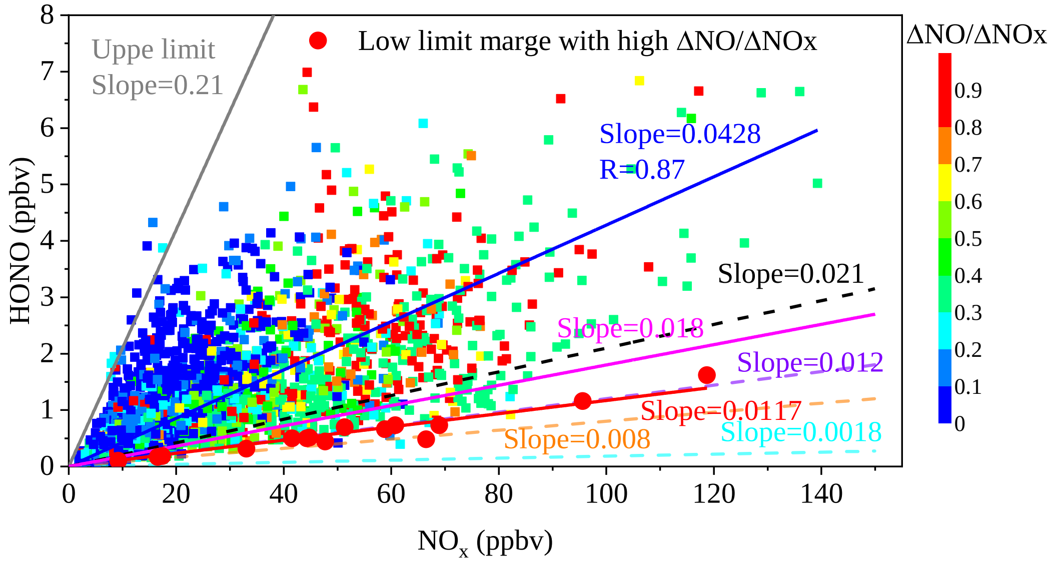

Figure S9. Correlation of measured HONO concentration with NO_x concentration.

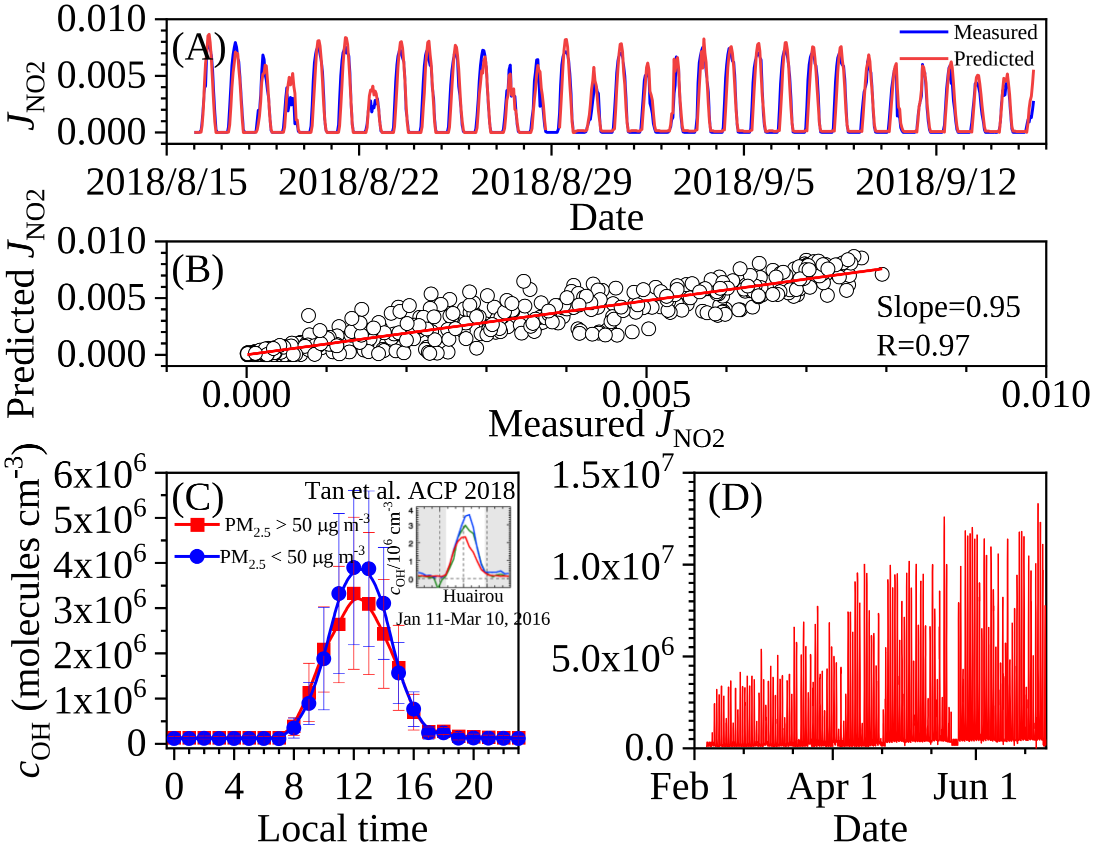

Figure S10. (A) Measured and predicted J_{NO2} and (B) the correlation between measured and predicted J_{NO2} from Aug. 15 to Sep. 16; (C) calculated diurnal curve of OH concentration based on J_{O1D} compared with that measured at Huairou (60 km northeast from BUCT) from Jan 11 to Mar 10, 2016; (D) OH concentrations estimated using $c_{OH}=J_{O1D}\times2\times10^{11}$(Tan et al., 2019).

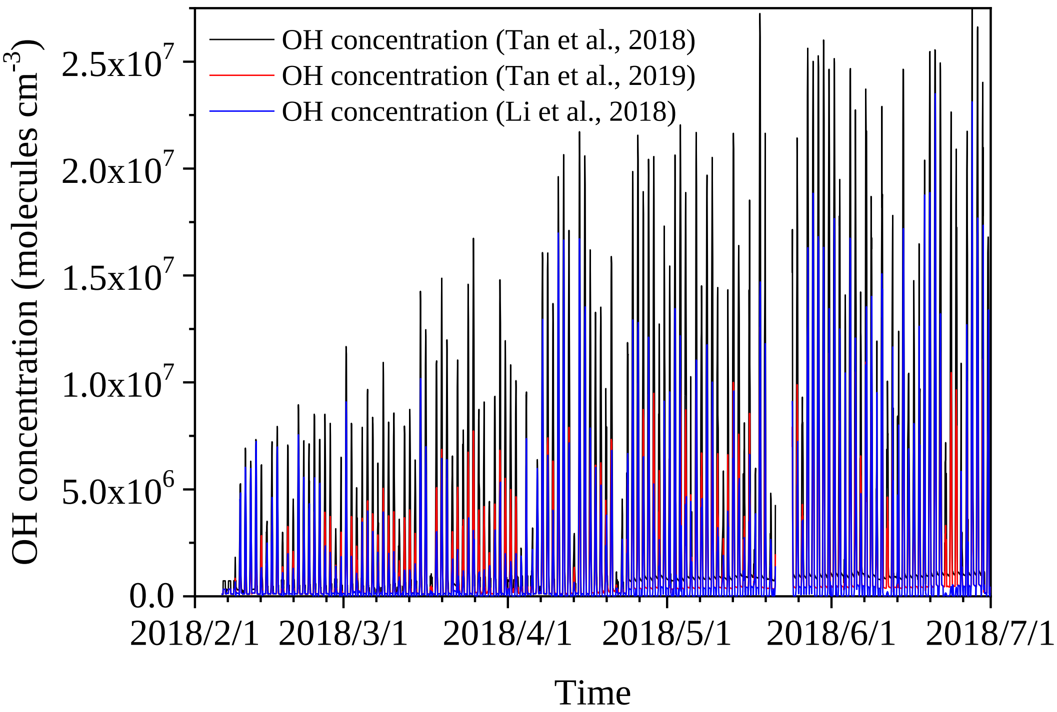

93

94 Fig. S11. Estimated OH concentration using different methods.

95

Supplementary tables

Table S1. ANOVA statistics analysis for the monthly mean fraction of the individual component in NR-$PM_{2.5}$ and HONO concentration.

Component	Fraction of NR-$PM_{2.5}$ (%) or Concentration of gaseous pollutants (ppbv)	Feb	Mar	Apr	May
Ammonium	Feb (12.2±2.9)				
	Mar (14.2±2.8)	Significant			
	Apr (14.0±4.0)	Significant	Not significant		
	May (11.6±4.6)	Not significant	Significant	Significant	
	Jun (12.2±5.2)	Not significant	Significant	Significant	Not significant
Chloride	Feb (7.7±6.1)				
	Mar (4.4±2.6)	Significant			
	Apr (1.1±1.2)	Significant	Significant		
	May (0.7±1.1)	Significant	Significant	Not significant	
	Jun (0.3±0.2)	Significant	Significant	Significant	Not significant
Nitrate	Feb (16.2±8.5)				
	Mar (26.7±8.8)	Significant			
	Apr (22.0±11.7)	Significant	Significant		
	May (17.3±11.8)	Not significant	Significant	Significant	
	Jun (16.7±12.8)	Not significant	Significant	Significant	Not significant
Organic	Feb (47.9±10.7)				
	Mar (45.9±10.2)	Not significant			
	Apr (46.5±14.2)	Not significant	Significant		
	May (52.9±17.0)	Not significant	Significant	Significant	
	Jun (52.6±18.7)	Significant	Significant	Significant	Not significant

Sulfate	Feb (16.0±9.1)				
	Mar (8.8±5.4)	Significant			
	Apr (16.4±8.2)	Not significant	Significant		
	May (17.5±6.6)	Significant	Significant	Not significant	
	Jun (18.2±8.0)	Significant	Significant	Significant	Not significant
BC	Feb (3.0±2.8)				
	Mar (4.6±3.1)	Significant			
	Apr (3.2±2.6)	Not significant	Significant		
	May (2.8±2.1)	Not significant	Significant	Not significant	
	Jun (2.6±1.5)	Significant	Significant	Significant	Not significant
HONO	Feb (0.73±0.70)				
	Mar (1.53±1.25)	Significant			
	Apr (1.38±1.35)	Significant	Not significant		
	May (1.31±1.00)	Significant	Significant	Not significant	
	Jun (1.35±0.80)	Significant	Significant	Not significant	Not significant
NOx	Feb (20.4±17.3)				
	Mar (40.5±24.0)	Significant			
	Apr (22.8±18.6)	Not significant	Significant		
	May (25.0±15.9)	Significant	Significant	Not significant	
	Jun (19.0±12.1)	Not significant	Significant	Significant	Significant
SO_2	Feb (3.8±3.3)				
	Mar (12.1±13.0)	Significant			
	Apr (2.8±2.4)	Significant	Significant		
	May (1.8±1.7)	Significant	Significant	Not significant	
	Jun (1.3±1.2)	Significant	Significant	Significant	Not significant
CO	Feb (959.6±554.6)				

	Mar (1075.0±571.8)	Significant			
	Apr (546.6±378.1)	Significant	Significant		
	May (554.1±336.9)	Significant	Significant	Not significant	
	Jun (583.4±286.2)	Significant	Significant	Not significant	Not significant
	Feb (22.6±14.6)				
	Mar (23.8±19.2)	Not significant			
O_3	Apr (43.5±29.0)	Significant	Significant		
	May (42.5±28.3)	Significant	Significant	Not significant	
	Jun (57.2±30.7)	Significant	Significant	Significant	Significant

Note: "Significant" or "Not significant" denotes that the difference of the monthly mean fractions or concentrations is significant or not significant at the 0.05 level.

Tab. S2. Mean concentrations of HONO and $PM_{2.5}$ in selected episodes

Episode No.	Duration	HONO (ppb)	Average $PM_{2.5}$ concentration	NR-$PM_{2.5}$ Concentration (%)									
				Chloride		Nitrate		Organic		Sulphate		Ammonium	
				(%)	($\mu g\ m^{-3}$)	(%)	($\mu g\ m^{-3}$)	(%)	($\mu g\ m^{-3}$)	(%)	($\mu g\ m^{-3}$)	(%)	($\mu g\ m^{-3}$)
1	Feb 2-5	0.38±0.28	9.3±4.5	4.0±2.3	0.26±0.39	12.3±5.6	0.80±1.17	51.1±10.0	2.68±3.00	20.6±9.2	0.69±0.24	12.0±3.2	0.54±0.49
2	Feb 8-9	0.90±0.72	44.5±3.5	6.3±2.9	1.59±1.46	15.8±7.9	4.20±3.87	49.9±4.8	9.63±7.64	17.3±8.8	2.31±1.42	10.8±1.0	2.14±1.69
3	Feb 10-12	0.31±0.40	9.0±0.8	5.2±3.5	0.18±0.22	6.8±3.9	0.30±0.44	48.6±10.6	1.75±1.72	28.1±11.5	0.74±0.38	11.2±2.5	0.35±0.23
4	Feb 16-19	1.38±0.86	101.5±26.8	15.5±4.2	9.04±4.94	25.0±4.1	13.15±7.73	32.2±3.8	18.21±8.25	14.4±3.7	7.82±4.39	12.9±1.5	6.85±3.78
5	Feb 21-24	0.64±0.58	24.3±7.0	5.5±4.1	0.60±0.51	14.9±6.3	1.80±1.38	56.3±10.0	5.83±2.94	11.8±5.0	1.17±0.67	11.6±2.8	1.24±0.77
6	Feb 25-28	0.87±0.64	108.8±42.9	5.2±1.4	2.94±1.97	27.1±3.9	15.3±8.77	42.5±6.8	22.83±9.68	10.4±3.8	6.44±5.78	14.7±1.8	8.34±5.30
7	Mar 2-3	1.41±0.84	120.0±47.0	8.3±2.2	4.23±1.72	26.5±4.8	15.29±9.44	44.4±6.2	23.40±10.49	7.2±1.9	4.36±3.37	13.5±1.9	7.74±4.76
8	Mar 8-10	1.36±0.89	88.7±34.2	4.8±1.8	1.87±1.09	28.3±5.2	11.00±6.20	43.0±7.0	15.65±7.15	9.0±2.8	3.10±1.42	14.9±2.0	5.58±2.92
9	Mar 11-14	2.27±1.68	170.3±75.4	3.5±0.9	2.48±1.32	34.8±4.3	28.32±19.09	36.8±5.0	27.90±15.78	8.1±1.8	6.60±4.72	16.8±1.5	13.57±8.99
10	Mar 16-19	1.88±1.38	66.0±25.7	3.8±1.7	1.99±1.18	30.2±6.3	17.40±12.45	35.9±2.8	20.87±10.52	13.5±5.1	7.00±4.92	16.5±1.0	9.17±5.86
11	Mar 21-23	1.41±0.72	83.7±22.1	5.3±2.8	2.54±2.30	31.5±3.8	12.23±5.22	45.1±6.7	18.02±5.46	4.4±1.0	1.67±0.92	13.7±1.6	5.38±2.08
12	Mar 25-27	2.22±1.34	129.5±51.9	2.0±0.7	0.94±0.64	35.3±3.6	16.32±9.90	41.5±5.4	20.46±10.18	5.7±1.2	2.56±1.68	15.6±1.6	7.11±4.37

Table S3. The summary of the HONO/NOx ratio from vehicles in this study and the reported emission ratio of HONO/NOx from vehicles in China.

No.	Time	$\Delta NO/\Delta NO_x$	$R_{\Delta NO/\Delta NOx}$	$\Delta HONO/\Delta NO_x$	$R_{\Delta HONO/\Delta NOx}$
1	2018/2/6 5:00-8:00	1.00	0.99	1.3%	0.92
2	2018/2/8 5:00-8:00	0.94	0.99	1.8%	0.96
3	2018/3/3 5:00-8:00	0.98	0.99	2.4%	0.96
4	2018/3/13 5:00-8:00	1.00	0.99	1.4%	0.86
5	2018/4/15 5:00-7:00	0.82	0.97	2.3%	0.99
Mean		0.95±0.08	-	1.8±0.5%	-

Time	Place	Methods	$\Delta HONO/\Delta NO_x$		Reference
			Range	Mean	
2015/9/1-2016/8/31	Ji'nan, Shandong	Empirical analysis of field data	0.19%-0.87%	0.53±0.20%	(Li et al., 2018)
2011/8/3-2012/5/31	Hongkong	Empirical analysis of field data	0.5%-1.6%	1.2±0.4%	(Xu et al., 2015)
2015/3/11-2015/3/21	Hongkong	Tunnel experiment	-	1.24±0.35%	(Liang et al., 2017)
2014	Beijing	Tunnel experiment	-	2.1%	(Yang et al., 2014)
2017	Beijing	Chassis dynamometer test	0.03%-0.42%	0.18%	(Liu et al., 2017)
2016/12/16-2016/12/24	Beijing	Empirical analysis of field data	-	1.3%	(Zhang et al., 2018)
2016/12/7-2016/12/13	Beijing	Low limit correlation of field data	-	1.41%	(Meng et al., 2019)
2018/2/1-2018/6/30	Beijing	Low limit correlation of field data	-	1.17%	This study
2018/2/1-2018/6/30	Beijing	Empirical analysis of field data	1.3-2.4%	1.8±0.5%	This study

References:

Fröhlich, R., Cubison, M. J., Slowik, J. G., Bukowiecki, N., Prévôt, A. S. H., Baltensperger, U., Schneider, J., Kimmel, J. R., Gonin, M., Rohner, U., Worsnop, D. R., and Jayne, J. T.: The ToF-ACSM: a portable aerosol chemical speciation monitor with TOFMS detection, Atmos. Meas. Tech., 6, 3225-3241, 10.5194/amt-6-3225-2013, 2013.

Li, D., Xue, L., Wen, L., Wang, X., Chen, T., Mellouki, A., Chen, J., and Wang, W.: Characteristics and sources of nitrous acid in an urban atmosphere of northern China: Results from 1-yr continuous observations, Atmos. Environ., 182, 296-306, https://doi.org/10.1016/j.atmosenv.2018.03.033, 2018.

Liang, Y., Zha, Q., Wang, W., Cui, L., Lui, K. H., Ho, K. F., Wang, Z., Lee, S.-c., and Wang, T.: Revisiting nitrous acid (HONO) emission from on-road vehicles: A tunnel study with a mixed fleet, J. Air Waste Manage. Assoc., 67, 797-805, 10.1080/10962247.2017.1293573, 2017.

Liu, Y., Lu, K., Ma, Y., Yang, X., Zhang, W., Wu, Y., Peng, J., Shuai, S., Hu, M., and Zhang, Y.: Direct emission of nitrous acid (HONO) from gasoline cars in China determined by vehicle chassis dynamometer experiments, Atmos. Environ., 169, 89-96, 10.1016/j.atmosenv.2017.07.019, 2017.

Meng, F., Qin, M., Tang, K., Duan, J., Fang, W., Liang, S., Ye, K., Xie, P., Sun, Y., Xie, C., Ye, C., Fu, P., Liu, J., and Liu, W.: High resolution vertical distribution and sources of HONO and NO2 in the nocturnal boundary layer in urban Beijing, China, Atmos. Chem. Phys. Discuss., 2019, 1-34, 10.5194/acp-2019-613, 2019.

Tan, Z. F., Lu, K. D., Jiang, M. Q., Su, R., Wang, H. L., Lou, S. R., Fu, Q. Y., Zhai, C. Z., Tan, Q. W., Yue, D. L., Chen, D. H., Wang, Z. S., Xie, S. D., Zeng, L. M., and Zhang, Y. H.: Daytime atmospheric oxidation capacity in four Chinese megacities during the photochemically polluted season: a case study based on box model simulation, Atmos. Chem. Phys., 19, 3493-3513, 10.5194/acp-19-3493-2019, 2019.

Tong, S., Hou, S., Zhang, Y., Chu, B., Liu, Y., He, H., Zhao, P., and Ge, M.: Exploring the nitrous acid (HONO) formation mechanism in winter Beijing: direct emissions and heterogeneous production in urban and suburban areas, Faraday Discuss., 189, 213-230, 10.1039/c5fd00163c, 2016.

Williams, L. R., Gonzalez, L. A., Peck, J., Trimborn, D., McInnis, J., Farrar, M. R., Moore, K. D., Jayne, J. T., Robinson, W. A., Lewis, D. K., Onasch, T. B., Canagaratna, M. R., Trimborn, A., Timko, M. T., Magoon, G., Deng, R., Tang, D., de la Rosa Blanco, E., Prevot, A. S. H., and Worsnop, D. R.: Characterization of an aerodynamic lens for transmitting particles greater than 1 micrometer in diameter into the Aerodyne aerosol mass spectrometer, Atmos. Meas. Tech., 6, 3271-3280, 10.5194/amt-6-3271-2013, 2013.

Xu, Z., Wang, T., Wu, J., Xue, L., Chan, J., Zha, Q., Zhou, S., Louie, P. K. K., and Luk, C. W. Y.: Nitrous acid (HONO) in a polluted subtropical atmosphere: Seasonal variability, direct vehicle emissions and heterogeneous production at ground surface, Atmos. Environ., 106, 100-109, 10.1016/j.atmosenv.2015.01.061, 2015.

Yang, Q., Su, H., Li, X., Cheng, Y., Lu, K., Cheng, P., Gu, J., Guo, S., Hu, M., Zeng, L., Zhu, T., and Zhang, Y.: Daytime HONO formation in the suburban area of the megacity Beijing, China, Sci. China-Chem., 57, 1032-1042, 10.1007/s11426-013-5044-0, 2014.

Zhang, W., Tong, S., Ge, M., An, J., Shi, Z., Hou, S., Xia, K., Qu, Y., Zhang, H., Chu, B., Sun, Y., and He, H.: Variations and sources of nitrous acid (HONO) during a severe pollution episode in Beijing in winter 2016, Scie. Total Environ., 648, 253-262, 10.1016/j.scitotenv.2018.08.133, 2018.